Richtmyer-Meshkov mixing zone study by a multidirectional laser absorption technique

L. Houas, A. Touat, and G. Jourdan
Institut Universitaire des Systèmes Thermiques Industriels, CNRS umr 139, Université de Provence, case 321, Centre Saint Jérôme, 13397 Marseille Cedex 20, France
(Received 22 September 1994; revised manuscript received 19 May 1995)

Shock tube experiments have been undertaken in which a shock wave accelerates normally to an interface separating two gases of different densities leading to the formation of a three-dimensional mixing zone between the two gases. Assuming the mixing zone to be homogeneous and weakly dependent on the wall effects, an integrated monodirectional absorption technique had been previously carried out and average temperature and density evolutions were determined within it. But the mixing zone is really deformed by the wall effects and in consequence it is not homogeneous. Thus, to improve the diagnostic technique, the experimental setup has been modified so that the mixing zone is divided into nine identical homogeneous imaginary regions. Temperature and species concentration are determined through each region of the mixing zone by a multidirectional laser absorption technique in order to have some new information on the influence of the wall effects on the Richtmyer-Meshkov instability study in square-cross-section shock tubes. Furthermore, a better accuracy in the measurements of the mixing zone thickness is obtained from a discussion of the concentration profiles. The consequence is that previous results achieved with integrated techniques such as global Schlieren, shadograph, or monodirectional absorption methods seem to be strongly overestimated.

PACS number(s): 52.35.−g, 52.40.Nk

I. INTRODUCTION

One of the fundamental problems of nuclear fusion by inertial confinement is the creation and growth of a turbulent mixing zone between the shell material and the combustible. This mixing zone, connected to the hydrodynamic instability, called Richtmyer-Meshkov instability [1,2], contributes to the decrease of the efficiency of the nuclear reaction. Our shock tube experiment is the planar monodimensional simulation of this phenomenon. We study the evolution of such a mixing zone originated from the shock wave acceleration of a plane interface, which initially separates two gases of different densities. In the framework of the Richtmyer-Meshkov instability, most of the experimental measurements of the mixing zone thickness evolution [2–7] have been principally obtained from visualization techniques, which are integrated along the shock tube cross section. But the wall effects and the three-dimensional nature of the phenomenon alter the thickness measurements. Up to the present time, to obtain quantitative information, such as thermodynamic parameters, new techniques are undertaken such as x-ray densitometry [8,9], planar laser induced fluorescence [10], and, in our laboratory, monodimensional laser absorption [11]. The laser absorption techniques is based on the absorption coefficients of two characteristic vibrational-rotational lines of the CO_2 bending mode, which are measured using a continuous wave CO_2 laser as a diagnostic probe. Then, as detailed in the paper of Fortes, Ramdani, and Houas [11], average temperature and density profiles have been determined through a Richtmyer-Meshkov mixing zone that was supposed to be homogeneous. The technique was based on the paper of Wang [12] for the case of homogeneous mixing. In the present work, to improve the method, because the mixing zone is, of course, nonhomogeneous, we have divided the test chamber cross section into nine imaginary regions where, in each one, we consider the mixing to be homogeneous. However, there was nothing to make us expect that such a division was experimentally possible. Thus the present work and results prove that this original technique is available for the study of flows in square-cross-section shock tubes.

II. DIAGNOSTIC TECHNIQUE

A. Laser absorption principle of measurement

The laser absorption principle of measurement has been previously described in the paper by Fortes, Ramdani, and Houas [11]. Thus, in the present work, we give only a brief summary, necessary for the understanding of the experimental setup and the data process.

The absorption coefficient α depends on the temperature T and the density ρ at a determinated frequency ν of the absorbing medium.

$$\alpha_\nu = f(T, \rho_{CO_2}, \nu) .$$

With two measurements at two different frequencies, the resolution of a system of two equations with two unknowns (temperature and density) allows the determination of mean temperature and density profiles within the medium

$$\alpha_1 = \alpha_{\nu_1}(T, \rho_{CO_2}, \nu_1) ,$$

$$\alpha_2 = \alpha_{\nu_2}(T, \rho_{CO_2}, \nu_2) .$$

The calculation of the absorption coefficient is made with a Voigt profile hypothesis for the CO_2 laser line. This expression also takes into account the CO_2 hot band absorption and has been defined by [11]

$$\alpha_\nu(\rho,T)=\frac{8\pi^3\nu_0}{3hc}\frac{a}{\pi\Delta\nu_D}\left[\frac{\ln 2}{\pi}\right]^{1/2}\times g(j)|R_{12}|^2 Qv^{-1}|R_{j\to j\pm1}|^2\rho_{CO_2}\times\int_{-\infty}^{+\infty}\frac{\exp(-y^2)}{a^2+(x-y)^2}dy\sum_i\alpha(j_i,T)\ ,$$

with

$$\alpha(j_i,T)=\frac{hc}{KT}\left\{b_1\exp\left[\frac{-b_1 j_i(j_i+1)hc}{KT}-\frac{\theta_1}{T}\right]-b_2\exp\left[\frac{-b_2(j_i+j')(j_i+j'+1)hc}{KT}-\frac{\theta_3}{T}\right]\right\}\times\left\{1+\frac{1}{1+4\left[\frac{k_i}{\Delta\nu_c}\right]^2}\frac{|R'_{12}|^2}{|R_{12}|^2}\right\}\ ,$$

where ρ and T are the density and temperature of CO_2, respectively. The different used symbols are ν_0, the frequency of CO_2 laser line; $|R_{12}|^2$, a spectral characteristic equal to 1.37×10^{-39} ergs cm^3 given by Strilchuk and Offenberger [13]; j, the rotational number;

$$|R_{j\to j\pm1}|^2=\begin{cases}\dfrac{j+1}{2j+3} & \text{for an } R \text{ line}\\ \dfrac{j}{2j-1} & \text{for a } P \text{ line,}\end{cases}$$

$$Qv^{-1}=\left[1-\exp\left[-\frac{\theta_1}{T}\right]\right]\left[1-\exp\left[-\frac{\theta_2}{T}\right]\right]^2\times\left[1-\exp\left[-\frac{\theta_3}{T}\right]\right]\ ,$$

the vibrational partition function of CO_2; a, the Voigt coefficient ($2<a<4$), θ_i, the ith mode characteristic temperature; j_i, the rotational number of the ith hot band ($j'=0$ for an R line and $j'=1$ and for a P line); k_i, the difference between the CO_2 laser line center and the corresponding hot band center; $|R'_{12}|^2$, the power of ith hot band ($i=0$ for the central band and then $k_i=0$), and $\Delta\nu_C$ and $\Delta\nu_D$ the collisional and the Doppler spectral widths, respectively.

B. Multidirectional laser measurement through a square cross section

In the case of a square cross section, Wang [12] showed that the directions of measurements must be carefully chosen and data must be solved in a proper order. Figure 1 shows the different laser cross beams in the nine regions with five different experimental configurations.

Using two different laser lines, ten runs are necessary

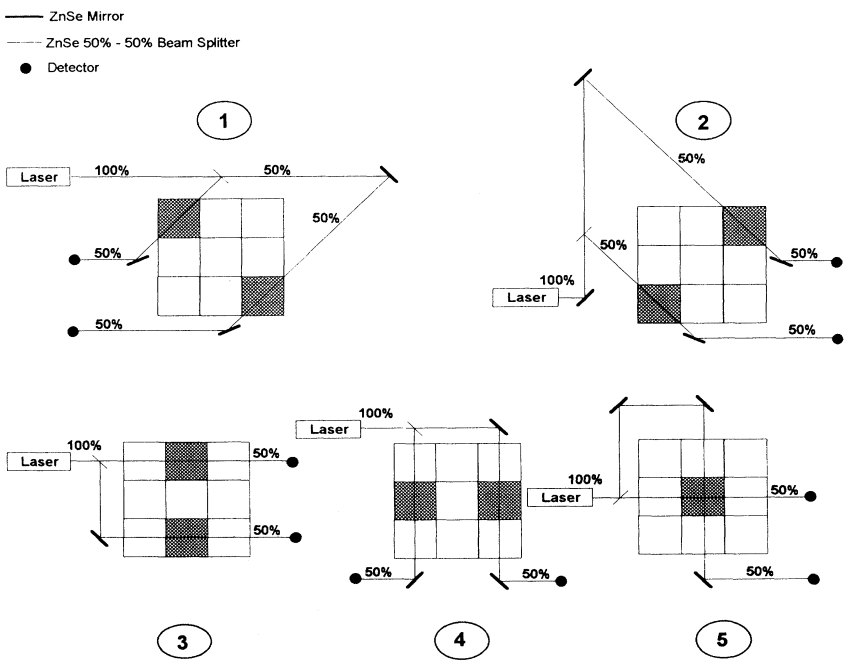

FIG. 1. Five different cross beam configurations through the shock tube cross section.

for obtaining one profile. Concerning the data process, similarly to Wang [12], we consider, in this paper, the optical thickness τ rather than the absorption coefficient (which was the case in Ref. [11]) defined by

$$\tau=\alpha L ,$$

where L is the length of the cross beam. The absorption of an isolated line (frequency ν) is related to the absorption coefficient α_ν by the relation

$$I=I_0\exp(-\alpha_\nu L) ,$$

where I_0 and I are the laser intensities (in watts) before and after absorption, respectively. Then

$$\tau=\ln\left[\frac{I_0}{I}\right] .$$

If the five laser beam directions are linearly independent, the total optical thickness through one optical way corresponds to the sum of all the optical thicknesses of the different probed regions (see Fig. 2)

$$\tau_{\text{total}}=\sum_i \tau_i .$$

In the present arrangement, regions (1,1), (3,3), (3,1), and (1,3) can be solved independently. From configuration 2, we have directly

$$\tau_{(1,3)}=\frac{\tau'_{(1,3)}}{\sqrt{2}} .$$

But the other regions (1,2), (3,2), (2,1), (2,3), and then (2,2) may be processed only in that order. For example, configuration 3 gives

$$\tau_{(3,2)}=\tau_{(3,1)(3,2)(3,3)}-[\tau_{(3,1)}+\tau_{(3,3)}] .$$

For the last case (2,2), we determine the absorbed energy through two different optical ways (Fig. 1, configuration 5) in order to evaluate the validity of the present diagnostic method

$$\tau_{(2,2)}=\tau_{(2,1)(2,2)(2,3)}-[\tau_{(2,1)}+\tau_{(2,3)}]$$

or

$$\tau_{(2,2)}=\tau_{(1,2)(2,2)(3,2)}-[\tau_{(1,2)}+\tau_{(3,2)}] .$$

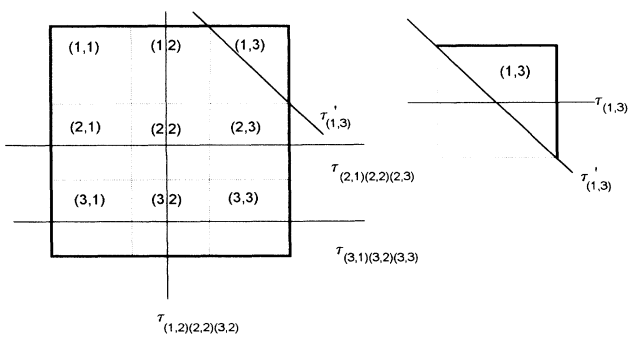

FIG. 2. Optical thicknesses for the laser cross beam measurements through the shock tube cross section for data process.

Preliminary results [14] have shown a significant symmetry in the four corners of the shock tube and near the walls; therefore, we suppose

$$\tau_{(1,1)}=\tau_{(1,3)}=\tau_{(3,1)}=\tau_{(3,3)} ,$$

$$\tau_{(1,2)}=\tau_{(2,1)}=\tau_{(2,3)}=\tau_{(3,2)} .$$

Then, considering these arrangements, the definitive absorption coefficient relations, for each case, are as follows: for the region in the corner

$$\alpha_{(1,3)}=\frac{3}{L_0\sqrt{2}}\ln\left[\frac{I'_{0,(1,3)}}{I'_{(1,3)}}\right] \text{ m}^{-1} ;$$

for the region near the wall,

$$\alpha_{(3,2)}=\frac{3}{L_0}\left\{\ln\left[\frac{I_{0(3,1)(3,2)(3,3)}}{I_{(3,1)(3,2)(3,3)}}\right]-\sqrt{2}\ln\left[\frac{I'_{0(1,3)}}{I'_{(1,3)}}\right]\right\} \text{ m}^{-1} ;$$

and for the region in the center,

$$\alpha_{(2,2)}=\frac{3}{L_0}\left\{\ln\left[\frac{I_{0(2,1)(2,2)(2,3)}}{I_{(2,1)(2,2)(2,3)}}\right]-2\ln\left[\frac{I_{0(3,1)(3,2)(3,3)}}{I_{(3,1)(3,2)(3,3)}}\right]2\sqrt{2}\ln\left[\frac{I'_{0(1,3)}}{I_{(1,3)}}\right]\right\} \text{ m}^{-1} ,$$

where L_0 represents the length of the shock tube cross section (8.5 cm). Thus the aim of this work is to obtain some information on the evolution of thermodynamic parameters within the mixing zone as far from the wall effects as possible and to try to evaluate the influence of the wall effects on the previous thicknesses measurements [3–7].

III. EXPERIMENTAL SETUP AND INITIAL CONDITIONS

A. Experimental setup

Experiments are performed in a double diaphragm shock tube of about 9 m total length. The test chamber is a 8.5×8.5 cm^2 square cross sections and its length is variable from 80 to 150 cm. The test gases are CO_2 because of its spectroscopic properties and argon or helium because they present no infrared absorption in the domain of our experiments and also because they allowed the study of the influence of the initial densities of the two gases that constitute the mixing (close for the CO_2-Ar mixing zone and different for CO_2-He one). They are initially separated by a thin plastic membrane (1.5 μm thick). Figure 3 presents a sketch of the general experimental setup with one of the five necessary configurations, where, for example, configuration 1 is presented. The simultaneous probe of two regions of the shock tube cross section is permitted by using ZnSe mirrors and beam splitters positioned along the incident laser beam optical way. The SAT C7 continuous wave CO_2 laser (8 W power, 2 mm beam diameter, and 3.1 mrad

divergence) is stabilized on a suitably chosen line, and Ge and ZnSe attenuators are used so that the incident laser beam power is less than 10 mW. The infrared detectors, type $Cd_xHg_{1-x}Te$ and centered at 10.6 μm, are cooled with liquid nitrogen. A frequency analyzer gives checks the band used ($P20$ and $R12$ lines). The absorption signals are recorded by a digitizing oscilloscope and processed by an IBM 486 DX 50-MHz personal computer for temperature and concentration calculations. Figure 4 gives an example of typical absorption signals for the CO_2-He test. Figure 4(a) represents the original absorption signal recorded in the center of the shock tube cross section from configuration 5. In this case, we observe that the plastic membrane particles (peaks behind the mixing zone) do not perturb the mixing zone, but, unfortunately, in some experiments these particles lie in the mixing zone and prevent the processing of experimental data. The presence of membrane pieces is also visible on the signal recorded near the shock tube wall [Fig. 4(b)] but not for the signal in the shock tube corner [Fig. 4(c)].

B. Initial conditions

Figures 5(a) and 5(b) give the experimental wave diagrams, where $x=0$ and $t=0$ correspond to the initial interface position and the instant of oscilloscope triggering, respectively. Absorption measurements have been realized at an abscissa of 550 mm from the initial position of the membrane, for two couples of test gases: CO_2-Ar and CO_2-He, with a Mach number of about 5 in the CO_2, which corresponds to Mach numbers of 4.25 and 2.4 in argon and helium, respectively. The mixing zone velocities behind the shock are 1100 m/s for the CO_2-Ar case and 1485 m/s for the CO_2-He one. Before running the experiment, both parts of the experimental chamber are pumped to a vacuum of 4×10^{-2} Torr and then filled with the two test gases. The same initial pressure of the gases on both sides of the plastic membrane is about 2000 Pa in order to prevent from any large initial bulge [15] and the use of two gas pairs CO_2-Ar and CO_2-He, allows us to analyze the influence of the Atwood number, defined by

$$\mathrm{At}=\frac{\rho_{(\mathrm{Ar\ or\ He})}-\rho_{CO_2}}{\rho_{(\mathrm{Ar\ or\ He})}+\rho_{CO_2}},$$

where ρ_i is the density of the gas i (i=Ar or He) taken just after the shock passage. Thus the correspondent Atwood numbers are -0.34 and -0.83 for the CO_2-Ar and CO_2-He cases, respectively.

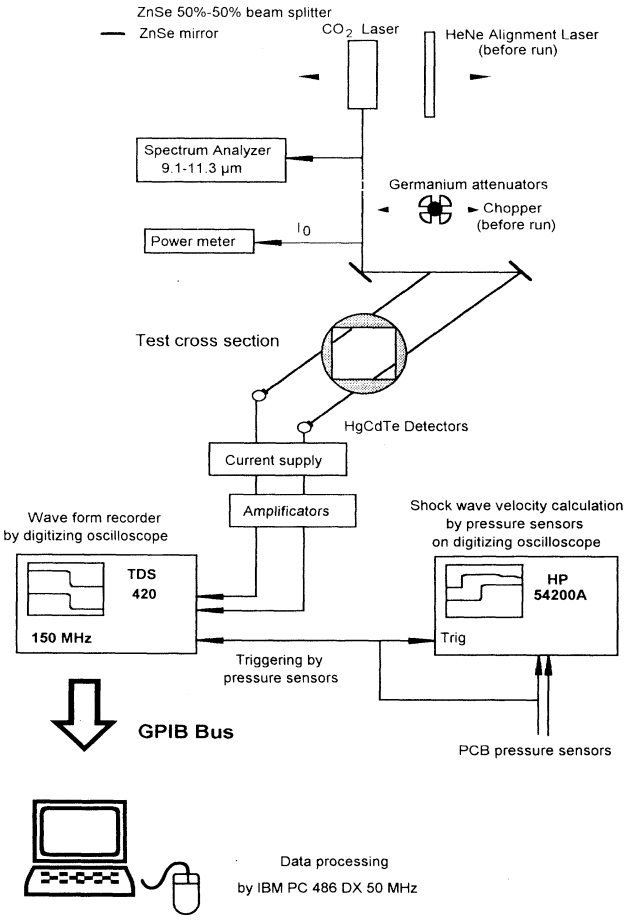

FIG. 3. Scheme of the experimental setup.

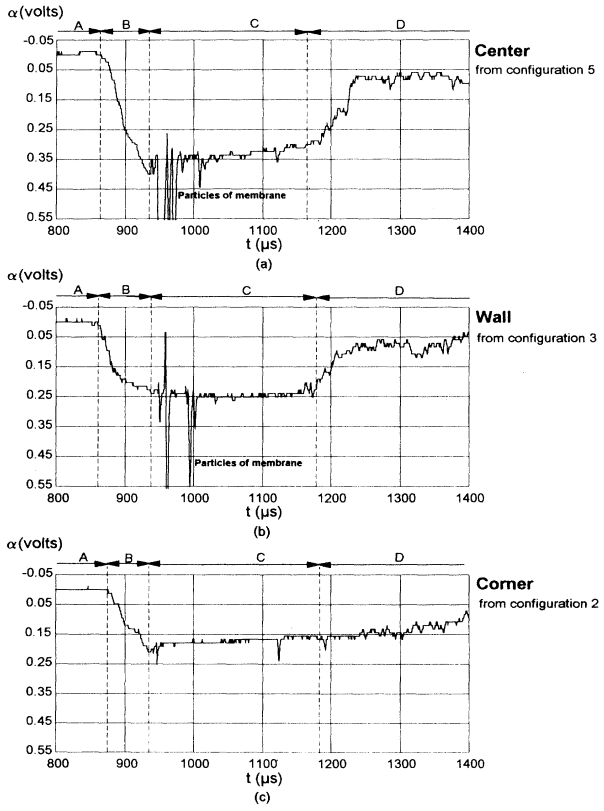

FIG. 4. Example of absorption signals for the CO_2-He mixing zone (a) in the center, (b) near the wall, and (c) of the shock tube cross section. *A*, *B*, *C*, and *D* correspond to the pure helium behind the incident shock, the mixing zone, the CO_2 behind the mixing zone, and the driver gas, respectively.

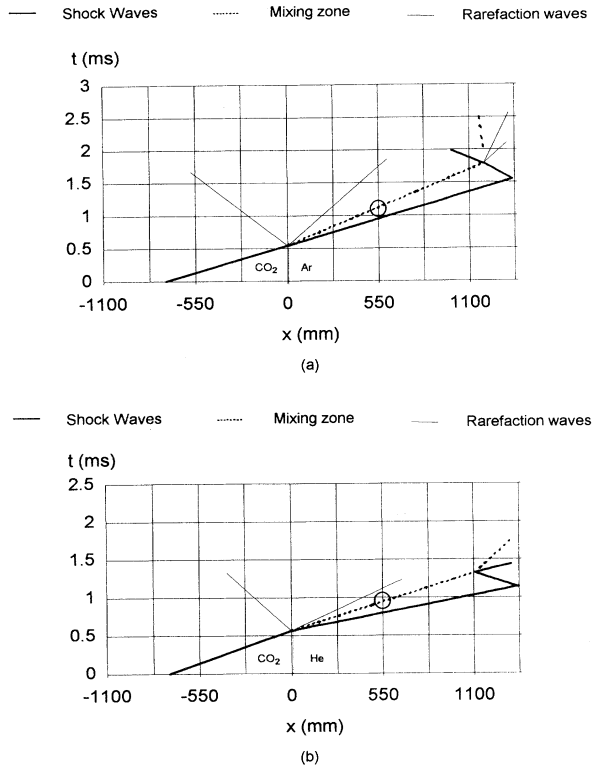

FIG. 5. Experimental wave diagrams: (a) the CO_2-Ar case and (b) the CO_2-He case.

IV. RESULTS AND DISCUSSION

Figures 6 and 7 present the normalized temperature and the CO_2 mass concentration evolutions within the Co_2-Ar and CO_2-He mixing zones. As preliminary results [14] have shown that the mixing zone presents a significant symmetry in the four corners of the shock tube and near the walls, we give, in this paper, only the results obtained in one corner, near one wall, and in the center of the tube.

The normalized temperatures T^* for the two tested mixing zones are presented in Fig. 6, where we have defined T^* by $T^*=(T-T_{CO_2})/(T_X-T_{CO_2})$ with $X=$Ar or He. In the center, the influence of shock tube walls seems to be negligible and the associated profiles are almost linear. Near the walls, the influence of the boundary layer, probably already turbulent for the CO_2-Ar mixing zone and probably laminar for the CO_2-He one, and the corner effects could explain the different temperature profiles in the first case and the more similar ones for the CO_2-He mixing zone. Thus it is probable that in the first case the laser beam near the walls (see configurations 3 and 4 in Fig. 1) crossed close to the boundary layer and is farther from it in the CO_2-He case. Presently, in the corner, the complex superposition of two boundary layers does not warrant the correct explanation of the results about the temperature profiles. Except for the center, which is far from the walls effects, we have found the temperature profiles difficult to discuss.

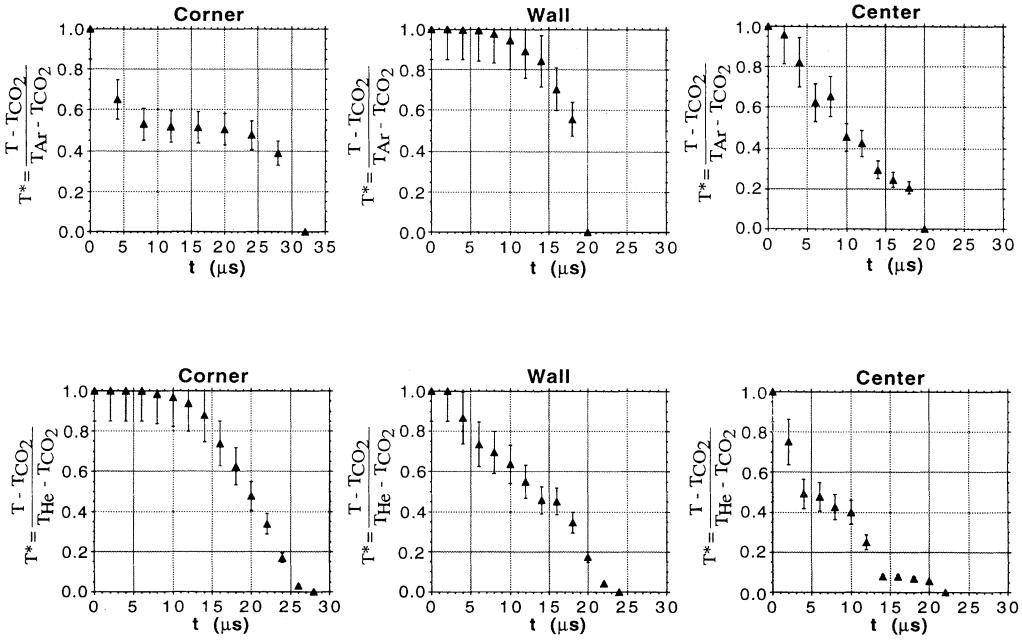

FIG. 6. Mixing zone normalized temperature evolutions in the corners, near the walls, and in the center of the shock tube: (a) the CO_2-Ar case and (b) the CO_2-He case.

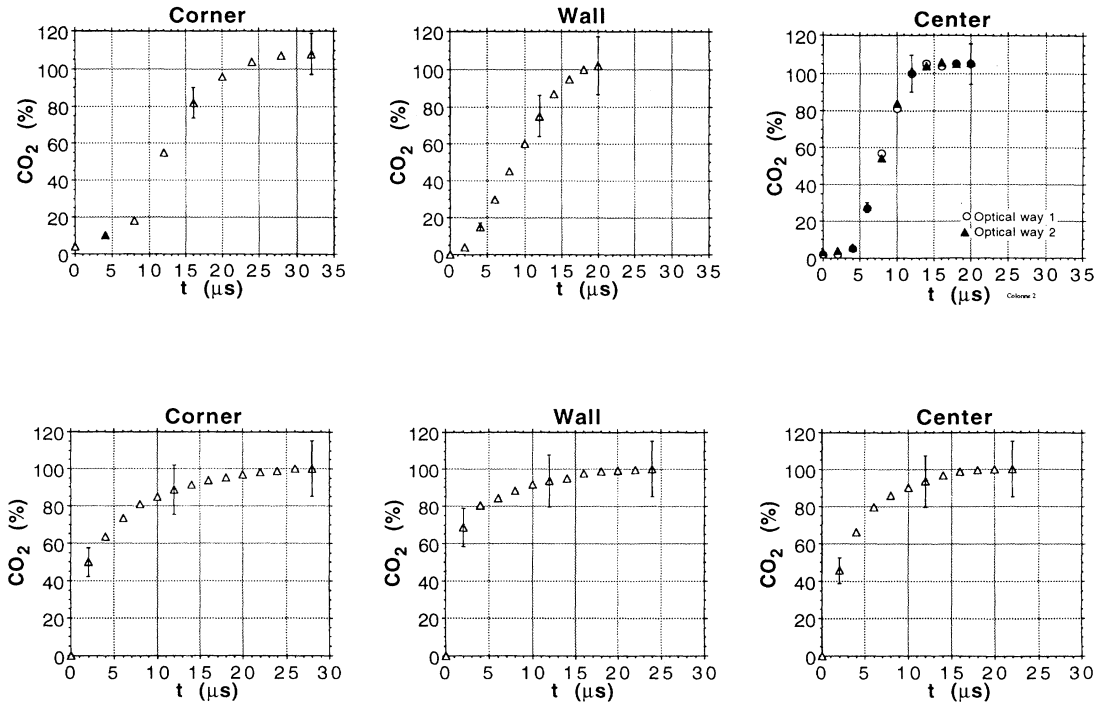

FIG. 7. Mixing zone CO_2 mass concentration evolutions in the corners, near the walls, and in the center of the shock tube: (a) the CO_2-Ar case and (b) the CO_2He case.

Concerning the CO_2 mass concentration evolutions, the two profiles obtained in the center for two different optical ways within the CO_2-Ar mixing zone [see Fig. 7(a)] are very similar and then validate the multidirectional diagnostic laser method. The different profiles obtained in each zone give some information about the influence of the boundary layer and the three-dimensional aspect of the turbulent mixing zone. Effectively, the mixing zone thickness is not homogeneous. As we can see, the thickness of the CO_2-Ar mixing zone is about 35 mm in the corner, 23 mm near the wall, and 22 mm in center of the shock tube cross section. It is the same for the CO_2-He case. We obtain 41 mm in the corner, 35 mm near the wall, and the 32 mm in the center.

The shape of each concentration profile curve in the center of the tube can be divided in three different regions. In the first one, which corresponds to about 5% (for the CO_2-He mixing zone) to 20% (for the CO_2-Ar case) of the total thickness of the mixing zone, the presence of the monoatomic gas in the mixing zone seems to be preponderant. The third region, about 40% for the two tested mixing zones, shows a preponderance of CO_2 since in this region we obtain more than 95% of the CO_2 mass concentration. In the second region, which is between the first and the third (approximately half of the mixing zone thickness for the two cases), we observe a variation of the concentration from 5% to 95%. In our opinion, this region corresponds to the mixing zone far from the deformation due to the wall effects. With these considerations, we can conceive of two possible three-dimensional aspects of the mixing zone shape in the shock tube, which are compatible with the concentration profiles and point out the wall effects: the mixing zone develops between two regions that are directly governed by the wall effects as schematically shown in Fig. 8. One can suppose that the deformation of the mixing zone, which can be deduced from the concentration profiles in the center, is more important in the CO_2-Ar case than in the CO_2-He one. This may show that the wall effects are more important in the first case. Thus, according to the hypothesis presented above, the thickness of the CO_2-Ar and CO_2-He mixing zones in the center of the shock tube would be about 10 mm (instead of 22 mn) and 16 mm (instead of 35 mm), respectively. However, knowing the exact value of the mixing zone thickness, which is correlated to the Richtmyer-Meshkov instability, is of course difficult because the estimation of the part of the mixing that had been stretched out to the shock tube walls remains very difficult. We can say only that the real value of the thickness of the mixing zone induced by the Richtmyer-Meshkov instability and without the influence of the wall effects is included between these two values and probably closer to the smallest one for a large shock tube cross-section measurements.

A direct comparison of previous thickness measurements using other integrated techniques is presented in Fig. 9. The compared diagnostic methods are Schlieren visualizations [2–6,16], CO_2 emission [17], and monodirectional laser absorption [11]. The evolution of the thickness of the mixing zone is plotted for the CO_2-Ar [Fig. 9(a)] and CO_2-He [Fig. 9(b)] cases versus the time for the same initial conditions. As we can see, if we com-

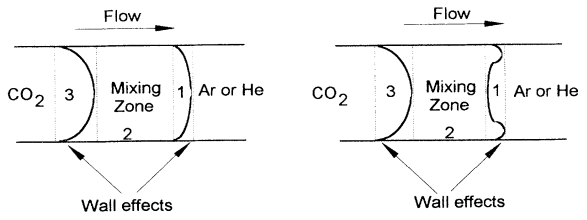

FIG. 8. Schemes of the different possible shapes of the mixing zone.

pare all the integrated techniques presented, the value of the mixing zone thickness is approximately independent of the diagnostic method. It is the same if we consider the total signal obtained in the center of shock tube with the present technique (see Fig. 7). However, if we deduce the thickness of the mixing zone from the concentration profile, we obtain in both cases a value of the mixing zone thickness that has to be corrected by a factor of about 0.5.

As a consequence, in comparison to the present technique, thickness measurements obtained from integrated methods could be strongly overestimated due to the wall effect deformation of the mixing zone. However, the present results can be used for an improvement of some existing [18–21] or future two-dimensional codes for a better understanding of the Richtmyer-Meshkov instability in fluids dynamics.

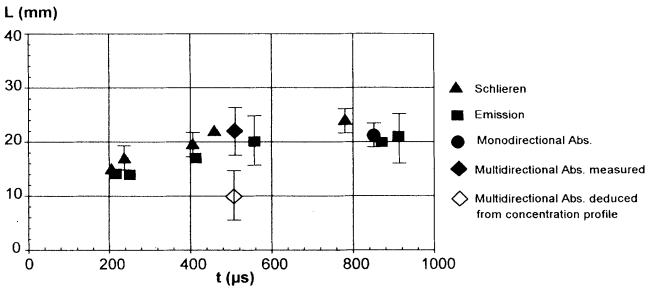

(a)

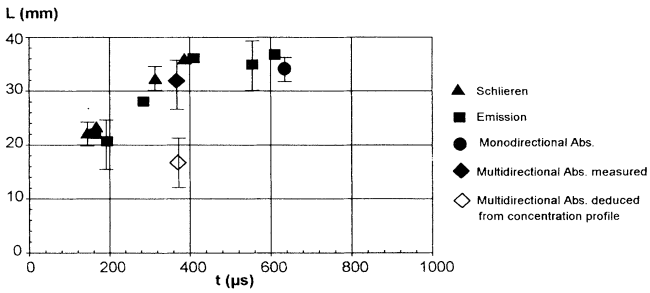

(b)

FIG. 9. Comparison of previous mixing zone thickness measurements using other integrated techniques with the multidirectional laser absorption method: (a) the CO_2-Ar case and (b) the CO_2-He case.

V. CONCLUSION

A multidirectional laser absorption technique has been applied for the study of Richtmyer-Meshkov mixing zone deformation induced by shock tube wall effects. Concentration and normalized temperature profiles obtained within different regions of the shock tube cross section give information on the deformation of the mixing zone due to the wall boundary layer and shock tube corners effects. Pointing out these disruptive phenomena was not possible using the monodimensional laser absorption method. These profiles constitute a data basis for future Richtmyer-Meshkov instability, numerical simulation, two-dimensional codes. Furthermore, in comparison with direct thickness measurements by previous integrated techniques, it has been shown that the present method is able to provide more accurate thickness measurements of the mixing zone, based on the interpretation of the concentration evolution within the mixing zone itself. A consequence is that previous thickness measurements with integrated methods all along the shock tube cross section could be greatly overestimated.

ACKNOWLEDGMENT

This work is supported by the Centre d'Etudes Nucléaires de Vaujours-Moronvilliers, Contract No. 304 844/00/D1.

[1] R. D. Richtmyer, Commun. Pure Appl. Math. **13**, 297 (1960).

[2] Y. Y. Meshkov, NASA Report No. TT F-13,074, 1970 (unpublished).

[3] V. A. Andronov, S. M. Bakhrakh, E. E. Meshkov, V. N. Mokhov, V. V. Nikiforov, A. V. Pevnitskii, and A. I. Tolshmyakov, Sov. Phys. JETP **44**, 424 (1976).

[4] S. G. Zaitsev, E. V. Lazareva, V. V. Chernukha, and V. M. Belyaev, Sov. Phys. Dokl. **30**, 579 (1985).

[5] M. Brouillette and B. Sturtevant, Physica D **37**, 248 (1989).

[6] C. Cavailler, H. Croso, P. Gandeboeuf, J. F. Haas, and G. Rodriquez, in *Proceedings of the Third International Workshop on the Physics of Compressible Turbulent Mixing,* edited by N. Wilke *et al.* (CEA-DAM, Royaumont, 1991), p. 27.

[7] L. Houas, I. Chemouni, A. Touat, and R. Brun, in *Proceedings of the Third International Workshop on the Physics of Compressible Turbulent Mixing,* (Ref. [6]), p. 127.

[8] R. Bonazza and B. Sturtevant, in *Proceedings of the Fourth International Workshop on the Physics of Compressible Turbulent Mixing,* edited by P. F. Linden, D. L. Youngs, and S. B. Dalziel (Cambridge University Press, Cam-

bridge, England, 1993), p. 194.
[9] G. Rodriquez, I. Galametz, H. Croso, and J. F. Haas, in *Proceedings of the Fourth International Workshop on the Physics of Compressible Turbulent Mixing* (Ref. [8]), p. 260.
[10] J. W. Jacobs, D. G. Jenkins, D. L. Klein, and R. F. Benjamin, in *Proceedings of the Fourth International Workshop on the Physics of Compressible Turbulent Mixing* (Ref. [8]), p. 223.
[11] J. Fortes, A. Ramdani, and L. Houas, Phys. Rev. E **50**, 3041 (1994).
[12] J. Y. Wang, Appl. Opt. **15**, 768 (1976).
[13] A. R. Strilchuk and A. A. Offenberger, Appl. Opt. **13**, 2643 (1974).
[14] A. Touat, I. Chemouni, G. Jourdan, L. Labracherie, and L. Houas, in *Proceedings of the 19th International Symposium on Shock Tubes and Waves,* edited by R. Brun and L. Z. Dumitrescu (Springer-Verlag, Berlin, 1993).
[15] L. Houas, A. Farhat, and R. Brun, Phys. Fluids **31**, 807 (1988).
[16] L. Houas, I. Chemouni, and A. Touat, in *Proceedings of the 18th International Symposium on Shock Tubes and Waves,* edited by K. Takayama (Springer-Verlag, Berlin, 1991), p. 319.
[17] L. Houas, R. Brun, and M. Hanana, AIAA J. **24**, 1254 (1986).
[18] D. Besnard, J. F. Haas, and R. M. Rauenzahn, Physica D **37**, 227 (1989).
[19] S. Gauthier and M. Bonnet, Phys. Fluids A **2**, 1685 (1990).
[20] K. O. Mikaelian, Phys. Fluids **2**, 592 (1990).
[21] K. O. Mikaelian, Phys. Rev. A **42**, 3400 (1990).